Proceedings of the XI DINAME, 28th February-4th March 2005, Ouro Preto - MG - Brazil


# VEHICLE MODELLING BY SUBSYSTEMS

**Georg Rill**

FH Regensburg, University of Applied Sciences, Galgenbergstr. 30, 93053 Regensburg

GeorgRill@aol.com

**Abstract.** *Computer simulations have become very popular in the automotive industry. In order to achieve a good conformity to field test sophisticated vehicle models are needed. A real vehicle incorporates many complex dynamic systems, like the drive train, the steering system and the wheel/axle suspension. On closer inspection some force elements such as shock absorbers and hydro-mounts turn out to be dynamic systems too. Modern vehicle models consist of different subsystems. Then, each subsystem may be modelled differently and can be tested independently. If some subsystems are available as a set of nested models of different complexity it is even possible to generate overall vehicle models which are well tailored to particular applications. But the numerical solution of coupled subsystems is not straight forward. This paper shows that by suitable interfaces and an implicit integration algorithm the overall vehicle model can be solved very effectively. The presented concept is realized in the product ve-DYNA applied world wide by automotive companies and suppliers.*

**Keywords.** *Vehicle Dynamics, Vehicle Model, Axle Modelling, Drive Train, Multibody Systems*

## 1. Modelling Concept

For dynamic simulation the vehicles are usually modelled by multi-body-systems (MBS), van der Jagt (2000). Usually the overall vehicle model is separated into different subsystems, Rauh (2003). Fig. 1 shows the components of a passenger car model which can be used to investigate handling and ride properties. The vehicle model consists of the vehicle framework

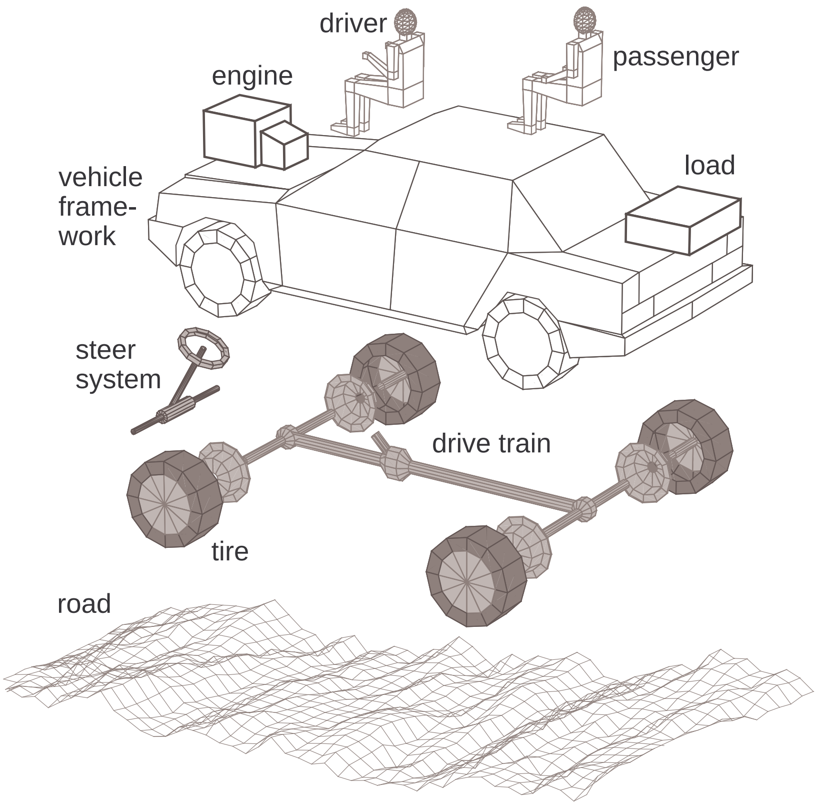


Figure 1: Vehicle Model Structure

and subsystems for the steering system and the drive train.

The vehicle framework represents the kernel of the model. It includes at least the module chassis and modules for the wheel/axle suspension systems. The vehicle framework is supplemented by modules for the load, an elastically suspended engine, and passenger/seat models. A simple load module just takes the mass and inertia properties of the load into account. To describe the sloshing effects of liquid loads dynamic load models are needed, Rill and Rauh (1992). The subsystems elastically suspended engine, passenger/seat and in heavy truck models a suspended driver's cabin can all be handled by the presented generic free body model. For standard vehicle dynamic analysis the chassis can be modelled by one rigid body. For applications where the chassis flexibility has to be taken into account a suitable flexible frame model is presented. Most wheel/axle suspension systems can be described by typical multi-body-systems elements like rigid bodies, links, joints and force elements, Rill (1994). Using a modified implicit Euler algorithm for solving the dynamic equations axle suspensions with compliancies and dry friction in the damper element can be handled without any problems, Rill (2004). Due to their robustness leaf springs are still a popular choice for solid axles. Leaf springs combine guidance and suspension properties which causes many problems in modelling, Fickers and Richter (1994). In this paper a leaf spring model is presented which overcomes this problems.

The steering system consists at least of the steering wheel, a flexible steering shaft and the steering box which may also be power-assisted. Neureder (2002) has developed a very sophisticated model of the steering system which includes compliancies, dry friction, and clearance.

Tire forces and torques have a dominant influence on vehicle dynamics. The semi-empirical tire model TMeasy has mainly been developed to meet both the requirements of user-friendliness and sufficient model accuracy, Hirschberg et. al. (2002). For special applications complex tire models like the FTire Model provided by Gipser (1998) can be used. The module tire also includes the wheel rotation which acts as input for the drive train model. The presented drive train model is generic. It takes lockable differentials into account, and it combines front wheel, rear wheel and all wheel drive. The drive train is supplemented by a module describing the engine torque. It may be modelled quit simply by a first order differential equation or by using the enhanced engine torque module en-DYNA developed by TESIS.

Road irregularities and variations in the coefficient of friction present significant impacts to the vehicle. A road model generating a two-dimensional reproducible random profile was provided by Rill (1990).

This modelling concept is realized with a MATLAB/Simulink® interface in the product ve-DYNA which also includes suitable models for the driver, TESIS.

## 2. Module Flexible Frame

### 2.1. Multi Body Approach to First Eigenmodes

The chassis eigenmodes of most passenger cars start at $f > 20\,Hz$. Hence, for standard vehicle dynamic analysis the chassis can be modelled as one rigid body. The lower chassis stiffness of trucks and pickups results in eigenmodes starting at $f \approx 10\,Hz$, Fig. 2. The first eigenmodes consist of chassis torsion and bending. This modes can be approximated by a

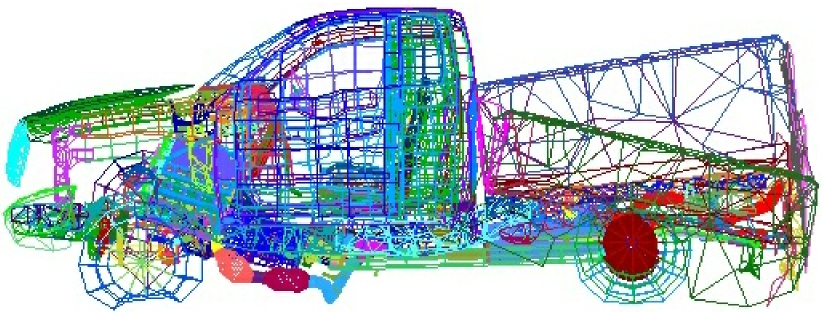

Figure 2: Chassis Eigenmode of a Pickup at $f = 11.2$ Hz

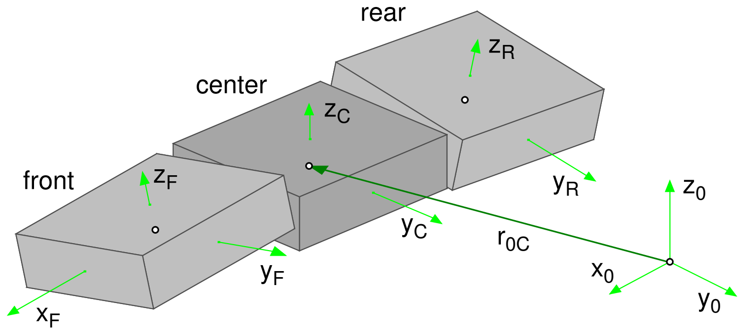


Figure 3: Flexible Frame Model

multi body chassis model where the chassis is divided into three parts, Fig. 3.

### 2.2. Free Body Motions

The position and orientation of the reference frame $x_C$, $y_C$, $z_C$ which is fixed to the center body with respect to the inertial frame $x_0$, $y_0$, $z_0$ is given by the rotation matrix

$$A_{0C} = \begin{bmatrix} \cos\gamma_{0C} & -\sin\gamma_{0C} & 0 \\ \sin\gamma_{0C} & \cos\gamma_{0C} & 0 \\ 0 & 0 & 1 \end{bmatrix} \begin{bmatrix} \cos\beta_{0C} & 0 & \sin\beta_{0C} \\ 0 & 1 & 0 \\ -\sin\beta_{0C} & 0 & \cos\beta_{0C} \end{bmatrix} \begin{bmatrix} 0 & 0 & 0 \\ 0 & \cos\alpha_{0C} & -\sin\alpha_{0C} \\ 1 & \sin\alpha_{0C} & \cos\alpha_{0C} \end{bmatrix} \tag{1}$$

and the position vector

$$r_{0C,0} = \begin{bmatrix} x_{0C} \\ y_{0C} \\ z_{0C} \end{bmatrix} , \tag{2}$$

where the comma separated subscript $_{,0}$ indicates, that the coordinates of the vector from 0 to $C$ are expressed in the inertial frame. The generalized coordinates roll, pitch and yaw angle $\alpha_{0C}$, $\beta_{0C}$, $\gamma_{0C}$ as well as the coordinates $x_{0C}$, $y_{0C}$, $z_{0C}$ of the vector $r_{0C,0}$ describe the free body motion of the vehicle.

### 2.3. Modal Coordinates

The motions of the front and rear body relative to the center body are small compared to the free body motions of the center part. Hence, the linearized rotation matrices

$$A_{CF} = \begin{bmatrix} 1 & -\gamma_{CF} & \beta_{CF} \\ \gamma_{CF} & 1 & -\alpha_{CF} \\ -\beta_{CF} & \alpha_{CF} & 1 \end{bmatrix} , \qquad A_{CR} = \begin{bmatrix} 1 & -\gamma_{CR} & \beta_{CR} \\ \gamma_{CR} & 1 & -\alpha_{CR} \\ -\beta_{CR} & \alpha_{CR} & 1 \end{bmatrix} , \tag{3}$$

and the position vectors

$$r_{CF,C} = r_{CF,K} + \begin{bmatrix} x_{CF} \\ y_{CF} \\ z_{CF} \end{bmatrix} , \qquad r_{CR,C} = r_{CR,K} + \begin{bmatrix} x_{CR} \\ y_{CR} \\ z_{CR} \end{bmatrix} \tag{4}$$

are used to describe the orientation and position of the front and rear body relative to the center part. The vectors $r_{CF,K}$ and $r_{CR,K}$ denote the initial position of the front and rear body.

The generalized coordinates

$$\begin{aligned} y_F &= [\ x_{CF},\ y_{CF},\ z_{CF},\ \alpha_{CF},\ \beta_{CF},\ \gamma_{CF}\ ]^T , \\ y_R &= [\ x_{CR},\ y_{CR},\ z_{CR},\ \alpha_{CF}\ \ \beta_{CR},\ \gamma_{CR}\ ]^T \end{aligned} \tag{5}$$

describe the motions of the front and rear body relative to the center body. This motions are now approximated by $n_M$ eigenmodes $e_1$, $e_2$, ... , $e_{n_M}$

$$y_F = \underbrace{\left[\, e_{F1},\ e_{F2},\ \cdots\ e_{Fn_M} \right]}_{E_F} \begin{bmatrix} m_1 \\ m_2 \\ \vdots \\ m_{n_M} \end{bmatrix} \quad \text{and} \quad y_R = \underbrace{\left[\, e_{R1},\ e_{R2},\ \cdots\ e_{Rn_M} \right]}_{E_R} \begin{bmatrix} m_1 \\ m_2 \\ \vdots \\ m_{n_M} \end{bmatrix} \tag{6}$$

where $m_1$, $m_2$, ..., $m_{n_M}$ are modal coordinates, and $E_F$ and $E_R$ are $6 \times n_M$ matrices containing the eigenmodes.

### 2.4. Generalized Coordinates

The flexible chassis is here modelled by 3 rigid bodies. The orientation and the position of the bodies are described by free body motions and modal coordinates

$$y_C = [\ x_{0C}\quad y_{0C}\quad z_{0C}\quad \alpha_{0C}\quad \beta_{0C}\quad \gamma_{0C}\quad m_1\quad m_2\quad \cdots\quad m_{n_M}\ ]^T , \tag{7}$$

where the 6 free body motions and the $n_M$ modal coordinates are collected in the vector $y_C$. The dimension of $y_C$ depends on the number $n_M$ of modal coordinates, $n_y = 6 + n_M$.

## 2.5. Equations of Motion

To generate the equations of motion Jordain's Principle with generalized speeds is used. For a multi body system consisting of $m$ rigid bodies it results in a set of two first order differential equations

$$\begin{aligned} K\,\dot{y} &= z\,, \\ M\,\dot{z} &= q\,. \end{aligned} \tag{8}$$

The kinematic matrix $K$ follows from the definition of the generalized speeds. The elements of the mass matrix $M$ are given by

$$M_{ij} = \sum_{k=1}^{m} \left\{ \frac{\partial v_{0k}^T}{\partial z_i}\, m_k\, \frac{\partial v_{0k}}{\partial z_j} + \frac{\partial \omega_{0k}^T}{\partial z_i}\, \Theta_k\, \frac{\partial \omega_{0k}}{\partial z_j} \right\}\,, \tag{9}$$

where $m_k$ is the mass and $\Theta_k$ the inertia tensor of body $k$. Finally, the components of the generalized forces and torques are defined by

$$q_i = \sum_{k=1}^{n} \left\{ \frac{\partial v_{0k}^T}{\partial z_i} \left[ F_{Ak} - m_k a_{0k}^R \right] + \frac{\partial \omega_{0k}^T}{\partial z_i} \left[ T_{Ak} - \Theta_k \alpha_{0k}^R - \omega_{0k} \times \Theta_k \omega_{0k} \right] \right\}\,, \tag{10}$$

where $F_{Ak}$, $T_{Ak}$ denote the forces and torques applied to body $k$ and $a_{0k}^R$, $\alpha_{0k}^R$ are remaining parts of the accelerations which do not depend on the derivatives of the generalized speeds.

## 2.6. Applied Forces and Torques

The forces and torques applied to the bodies can be written down as

$$\begin{aligned} F_C &= F_C^{ext} + F_{CF}^{cmp} + F_{CR}^{cmp}\,, \\ F_F &= F_F^{ext} - F_{CF}^{cmp}\,, \\ F_R &= F_R^{ext} - F_{CR}^{cmp} \end{aligned} \tag{11}$$

and

$$\begin{aligned} T_C &= T_C^{ext} + T_{CF}^{cmp} + T_{CR}^{cmp}\,, \\ T_F &= T_F^{ext} - T_{CF}^{cmp}\,, \\ T_R &= T_R^{ext} - T_{CR}^{cmp}\,, \end{aligned} \tag{12}$$

were the superscripts $^{ext}$ and $^{cmp}$ denote external and compliance forces and torques.

Applying Jordain's Principle one part within the equations of motion describes the whole chassis motion. For the whole chassis the compliance forces and torques are internal forces and therefore do not show up in the corresponding parts of the generalized force vector.

If we assume that the compliance forces and torques are proportional to the motions of the front and rear body then, we get

$$\begin{bmatrix} F_{CF}^{cmp} \\ T_{CF}^{cmp} \end{bmatrix} = c_{CF}\, y_F \quad \text{and} \quad \begin{bmatrix} F_{CR}^{cmp} \\ T_{CR}^{cmp} \end{bmatrix} = c_{CR}\, y_R\,, \tag{13}$$

were $c_{CF}$ and $c_{CR}$ are $6\times6$ stiffness matrices. The modal coordinate approximation Eq. (6) results in

$$\begin{bmatrix} F_{CF}^{cmp} \\ T_{CF}^{cmp} \end{bmatrix} = c_{CF}\, E_F \begin{bmatrix} m_1 \\ m_2 \\ \vdots \\ m_{nF} \end{bmatrix} \quad \text{and} \quad \begin{bmatrix} F_{CR}^{cmp} \\ T_{CR}^{cmp} \end{bmatrix} = c_{CR}\, E_R \begin{bmatrix} m_1 \\ m_2 \\ \vdots \\ m_{nF} \end{bmatrix}\,. \tag{14}$$

Within Jordain's Principle the compliance forces and torques are reduced to generalized forces which are calculated by

$$q_F^{cmp} = E_F^T\, c_{CF}\, E_F \begin{bmatrix} m_1 \\ m_2 \\ \vdots \\ m_{nF} \end{bmatrix} \quad \text{and} \quad q_R^{cmp} = E_R^T\, c_{CR}\, E_R \begin{bmatrix} m_1 \\ m_2 \\ \vdots \\ m_{nF} \end{bmatrix}\,, \tag{15}$$

where

$$E_F^T\, c_{CF}\, E_F = \begin{bmatrix} c_{F1} & 0 & \cdots & 0 \\ 0 & c_{F2} & \ddots & \vdots \\ \vdots & \ddots & \ddots & 0 \\ 0 & \cdots & 0 & c_{Fn_M} \end{bmatrix} \quad \text{and} \quad E_R^T\, c_{CR}\, E_R = \begin{bmatrix} c_{R1} & 0 & \cdots & 0 \\ 0 & c_{R2} & \ddots & \vdots \\ \vdots & \ddots & \ddots & 0 \\ 0 & \cdots & 0 & c_{Rn_M} \end{bmatrix} \tag{16}$$

are $n_M \times n_M$ stiffness matrices. which are defined by the modal stiffnesses $c_{F1}$, $c_{F2}$, ... $c_{Fn_M}$ and $c_{R1}$, $c_{R2}$, ... $c_{Rn_M}$. Thus, to describe the motions of a flexible chassis only some eigenmodes and modal stiffnesses have to be provided.

### 2.7. Results

Depending on the vehicle layout a flexible frame has a significant influence on the driving behavior, Fig 4. The rear axle

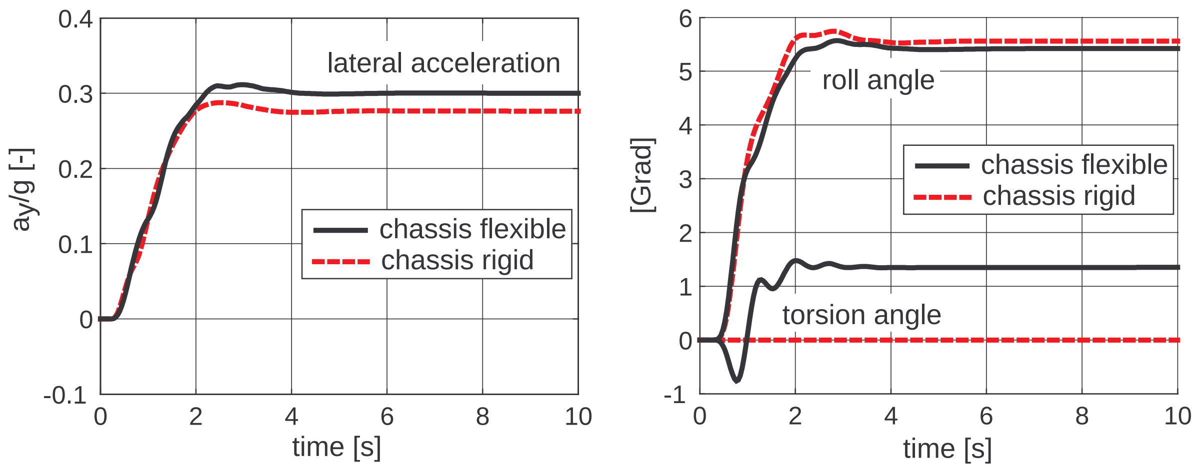


Figure 4: Step Input on Bus with rigid and flexible Frame

of the bus under consideration is guided by four links. The arrangement of the links generate here a steer effect which depends on the roll angle of the rear part of the chassis and therefor also on the torsional stiffness of the chassis.

## 3. Module Leaf Spring

### 3.1. Modelling Aspects

Poor leaf spring models approximate guidance and suspension properties of the leaf spring by rigid links and separate force elements, Matschinsky (1998). For realistic ride and handling simulations the deformation of the leaf springs must be taken into account.

Within ADAMS leaf springs can be modelled with sophisticated beam-element models, ADAMS/Chassis 12.0. But, according to Fickers (1994) it is not easy to take the spring pretension into account. To model the effects of a beam, ADAMS/Solver uses a linear 6-dimensional action-reaction force (3 translational and 3 rotational) between two markers. To provide adequate representation for the nonlinear cross section usually 20 elements are used to model one leaf spring. A subsystem consisting of a solid axle and two beam-element leaf spring models would have $f = 6 + 2 * (20 * 6) = 246$ degrees of freedom. In addition, the beam-element leaf spring model results in extremely stiff differential equations. This and the large number of degrees of freedom slow down the computing time significantly.

For real time applications the leaf springs must be modelled by a simple but still accurate model. Fig. 5 shows a model of a solid axle with leaf spring suspension which is typical for light truck rear axle suspension systems. There are no additional links. Hence, only the forces and torques generated by leaf spring deflections guide and suspend the axle.

The position of the axle center $A$ and the orientation of an axle fixed reference frame $x_A$, $y_A$, $z_A$ are described relative to a chassis fixed frame $x_B$, $y_B$, $z_B$ by the displacements $\xi$, $\eta$, $\zeta$ and the rotation angles $\alpha$, $\beta$, $\gamma$ which are collected in the $6 \times 1$ axle position vector

$$y_A = [\, \xi,\ \eta,\ \zeta,\ \alpha,\ \beta,\ \gamma \,]^T \ . \tag{17}$$

Similar to Fickers (1994) each leaf spring is modelled by five rigid bodies which are connected to each other by spherical joints, Fig. 5.

Each leaf spring is connected to the frame via the front leaf eye $X$. Furthermore each leaf spring is attached to the shackle at $Y$, and again to the frame at $Z$. In $C$ the center part of each leaf spring is rigidly connected to the axle. The front

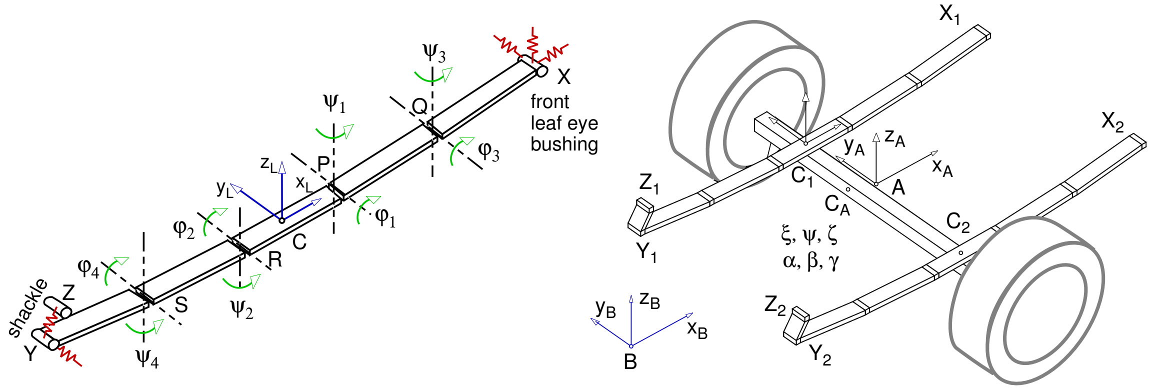


Figure 5: Axle Model with Leaf Spring Suspension

eye bushings are modelled by spring/damper elements in $x$-, $y$-, and $z$-direction. The shackles are modelled by radial and a lateral spring/damper elements. Within each leaf spring the angles $\varphi_1$, $\psi_1$, and $\varphi_2$, $\psi_2$ describe the motions of part $P$-$Q$ and part $R$-$S$ relative to the center part. The outer parts $Q$-$X$ and $P$-$Y$ perform their rotations, $\varphi_3$, $\psi_3$, and $\varphi_4$, $\psi_4$, relative to part $P$-$Q$ and part $R$-$S$. As each leaf spring element is considered as a rigid rod, the roll motions can be neglected. The angles are collected in $4\times 1$position vectors

$$y_{1F} = \left[\varphi_1^{(1)},\, \psi_1^{(1)},\, \varphi_3^{(1)},\, \psi_3^{(1)}\right]^T ; \quad y_{1R} = \left[\varphi_2^{(1)},\, \psi_2^{(1)},\, \varphi_4^{(1)},\, \psi_4^{(1)}\right]^T ; \tag{18}$$

$$y_{2F} = \left[\varphi_1^{(2)},\, \psi_1^{(2)},\, \varphi_3^{(2)},\, \psi_3^{(2)}\right]^T ; \quad y_{2R} = \left[\varphi_2^{(2)},\, \psi_2^{(2)},\, \varphi_4^{(2)},\, \psi_4^{(2)}\right]^T ; \tag{19}$$

where $y_{1F}$, $y_{2F}$ and $y_{1R}$, $y_{2R}$ describe the momentary shape of the front and the rear part of the left $(1)$ and the right $(2)$ leaf spring.

A fully dynamic description of a solid axle with two five link leaf spring models would result in $f = 6 + 2*8 = 22$ degrees of freedom. Compared to the beam-element model this is a really significant reduction.

But a dynamic description of the five link leaf spring model still includes some high frequent modes which will cause problems in the numerical solution of the equations of motion. As mass and inertia properties of the leaf spring model parts are small compared to the solid axle, a quasi static solution of the internal leaf spring deflection should be accurate enough within the overall vehicle model.

A quasi static solution provides the position vectors of the leaf spring parts as functions of the axle position vector, $y_{1F} = y_{1F}\,(y_A)$, $y_{1R} = y_{1R}\,(y_A)$, $y_{2F} = y_{2F}\,(y_A)$, $y_{2R} = y_{2R}\,(y_A)$. Hence, the sub system solid axle with two leaf springs has only $f = 6$ degrees of freedom.

### 3.2. Initial Shape and Pretension

At first it is assumed that the leaf spring is located in the $xz$-plane of the leaf spring fixed frame $x_L$, $y_L$, $z_L$ and its shape in the design position can be approximated by a circle which is fixed by the points $X$, $C$ and $Y$. By dividing the arc $X$-$Y$ into 5 parts of equal length the position of the links $P$, $R$, $S$, $Q$ and the initial values of the angles $\varphi_{01}$, $\psi_{01}$, $\varphi_{02}$, $\psi_{02}$, $\varphi_{03}$, $\psi_{03}$, $\varphi_{04}$, $\psi_{04}$ can be calculated very easily.

In design position each leaf spring is only preloaded by a vertical load which results in zero pretension forces in the $y_L$-direction, $F_{0B}^y = 0$, $F_{0S}^y = 0$ and zero pretension torques around the $z_l$-axis, $T_{0P}^z = 0$, $T_{0Q}^z = 0$, $T_{0R}^z = 0$, $T_{0S}^z = 0$. In addition the torques around the $x_l$-axis vanish, $T_{0P}^x = 0$, $T_{0Q}^x = 0$, $T_{0R}^x = 0$, $T_{0S}^x = 0$.

To transfer the vertical preload $F_0$ to the front eye bushing and the shackle, the joints $P$, $Q$, $R$, $S$ must provide torques around the $y_L$-axis, Fig. 6. The pretension forces in the front eye bushing $F_{0B}^x$, $F_{0B}^z$ and in the shackle $F_{0S}$, can easily be calculated from the equilibrium conditions of the five link leaf spring model,

$$\begin{aligned} F_{0B}^x + F_{0S}\, u_{YZ}^x &= 0\,, \\ F_{0B}^z + F_0 + F_{0S}\, u_{YZ}^z &= 0\,, \\ -r_{XC}^x\, F_0 + r_{XY}^z\, F_{0S}\, u_{YZ}^x - r_{XY}^x\, F_{0S}\, u_{YZ}^z &= 0\,, \end{aligned} \tag{20}$$

where $u_{YZ}$ is the unit vector in the direction of the shackle, and $r_{XY}^x$, $r_{XY}^z$ are the $x$ and $z$ components of the vector from pointing from $X$ to $Y$. The pretension torques in the leaf spring joints around the $y_l$-axis, $T_{0P}^y$, $T_{0Q}^y$, $T_{0R}^y$, $T_{0S}^y$ follow from

$$\begin{aligned} -T_{0P}^y + r_{PX}^z\, F_{0B}^x - r_{PX}^x\, F_{0B}^z &= 0\,, & -T_{0Q}^y + r_{QX}^z\, F_{0B}^x - r_{QX}^x\, F_{0Bz} &= 0\,, \\ T_{0R}^y + r_{RY}^z\, F_{0S}\, u_{YZ}^x - r_{RY}^x\, F_{0S}\, u_{YZ}^z &= 0\,, & T_{0S}^y + r_{SY}^z\, F_{0S}\, u_{YZ}^x - r_{SY}^x\, F_{0S}\, u_{YZ}^z &= 0\,, \end{aligned} \tag{21}$$

were $r_{ij}$, $i = P,\, Q,\, R,\, S$, $j = X,\, Y$ are vectors pointing from $i$ to $j$.

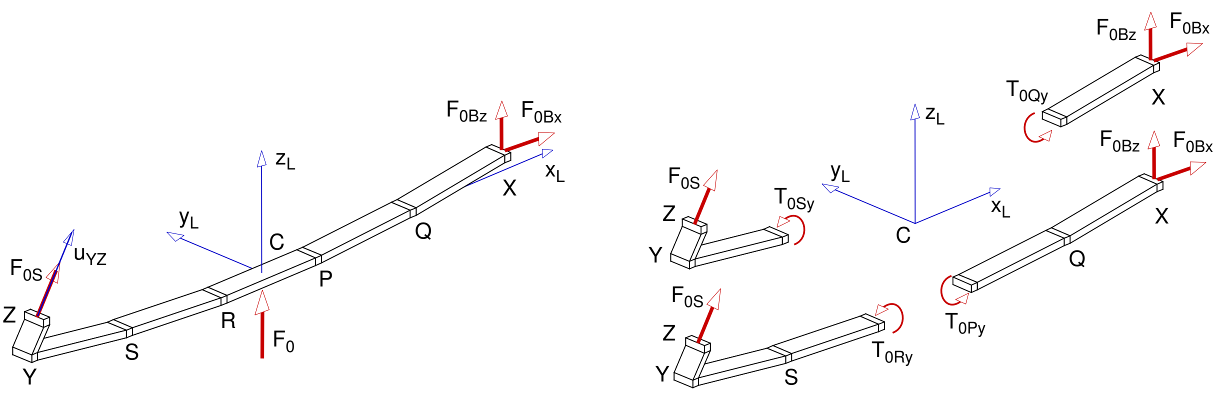


Figure 6: Pretension Forces and Torques

### 3.3. Compliance

The leaf spring compliance is defined in the design position by the vertical and the lateral stiffness, $c_V$ and $c_L$. In Fig. 7 a the leaf spring is approximated by a beam which is supported on both ends and is loaded in the center by the force $F$. The deflection $w$ and the force $F$ are related to each other by the stiffness $c$

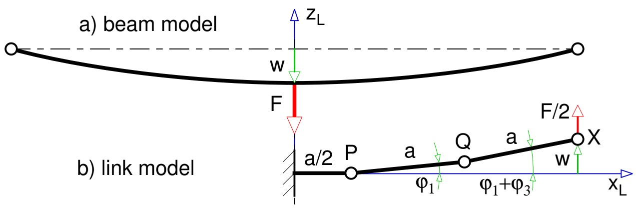


Figure 7: Leaf Spring Stiffness

$$F \;=\; c\,w\,. \tag{22}$$

If we transfer the beam model to the five link leaf spring model and look at the front half, Fig. 7b, then one gets

$$w \;=\; a\,\varphi_1 \;+\; a\;(\varphi_1 + \varphi_3)\;, \tag{23}$$

where $a$ is the length of one link, and small deflections in the $x_L$, $z_L$ plane were assumed. The torques around the $y_L$-axis in the joints $P$ and $Q$ would be proportional to the deflection angles $\varphi_1$ and $\varphi_3$

$$T_P^y \;=\; c_{\varphi_1}\,\varphi_1 \quad \text{and} \quad T_Q^y \;=\; c_{\varphi_3}\,\varphi_3\;. \tag{24}$$

The equilibrium condition results in

$$T_P^y \;=\; 2\,a\,\frac{F}{2} \quad \text{and} \quad T_Q^y \;=\; a\,\frac{F}{2}\;:\;. \tag{25}$$

The leaf spring bending mode due to a single force can be approximated very well by a circular arc. Hence, the relative angle between connected links is equal, $\varphi_1 = \varphi_3 = \varphi$ and Eq. (23) can be simplified to $w = 3\,a\,\varphi$ or $\varphi = \frac{w}{3\,a}$ From Eq. (24) and Eq. (25) it follows

$$c_{\varphi_1}\,\frac{w}{3\,a} \;=\; 2\,a\,\frac{F}{2} \quad \text{and} \quad c_{\varphi_3}\,\frac{w}{3\,a} \;=\; a\,\frac{F}{2}\;:\;. \tag{26}$$

Using Eq. (22) one finally gets

$$c_{\varphi_1} \;=\; 3\,a^2\,c_V \quad \text{and} \quad c_{\varphi_3} \;=\; \frac{3}{2}\,a^2\,c\,, \tag{27}$$

where the beam stiffness $c$ was replaced by the vertical leaf spring stiffness $c_V$. Assuming symmetry, the stiffnesses in the rear joints are given by $c_{\varphi_2} = c_{\varphi_1}$ and $c_{\varphi_4} = c_{\varphi_3}$. The stiffnesses around the vertical axis $c_{\psi_1}$, $c_{\psi_2}$, $c_{\psi_3}$ and $c_{\psi_4}$ can be calculated in a similar way. In this approach the torsional stiffness of the leaf spring is neglected.

### 3.4. Actual Shape

In an equilibrium position the energy of a flexible system achieves a minimum value, $E \to Min$. The energy of the five link leaf spring model is given by

$$\begin{aligned} E &= \tfrac{1}{2}\, w_X^T\, c_B\, w_X \;+\; \tfrac{1}{2}\, c_{\varphi_1}\, \varphi_1^2 + \tfrac{1}{2}\, c_{\psi_1}\, \psi_1^2 + \tfrac{1}{2}\, c_{\varphi_3}\, \varphi_3^2 + \tfrac{1}{2}\, c_{\psi_3}\, \psi_3^2 \\ &+\; \tfrac{1}{2}\, c_{\varphi_2}\, \varphi_2^2 + \tfrac{1}{2}\, c_{\psi_2}\, \psi_2^2 + \tfrac{1}{2}\, c_{\varphi_4}\, \varphi_4^2 + \tfrac{1}{2}\, c_{\psi_4}\, \psi_4^2 \;+\; \tfrac{1}{2}\, c_{SR}\, w_{SR}^2 + \tfrac{1}{2}\, c_{SL}\, w_{SL}^2 \,, \end{aligned} \tag{28}$$

where $w_X$ is the $3\times1$ displacement vector and $c_B$ is the $3\times3$ stiffness matrix of the front eye bushing, $w_{SR}$, $w_{SL}$ are the radial and lateral shackle displacements, and $c_{SR}$, $c_{SL}$ denote the corresponding stiffnesses.

According to Eq. (18) and Eq. (19), the actual shape of the leaf spring is determined by the position vectors $y_1 = [\,\varphi_1,\, \psi_1,\, \varphi_3,\, \psi_3\,]^T$ and $y_2 = [\,\varphi_2,\, \psi_2,\, \varphi_4,\, \psi_4\,]^T$. If the leaf spring energy becomes a minimum, then the following equations hold

$$\frac{\partial E}{\partial \varphi_1} = 0\,, \quad \frac{\partial E}{\partial \psi_1} = 0\,, \quad \cdots \quad \frac{\partial E}{\partial \varphi_4} = 0\,, \quad \frac{\partial E}{\partial \psi_4} = 0\,. \tag{29}$$

As the shackle displacements $w_{SR}$, $w_{SL}$ do not depend on $y_1$ and the front bushing displacement vector $w_X$ does not depend on $y_2$ the conditions in Eq. (29) form two independent sets of nonlinear equations $f_1(y_1,\, y_A) = 0$ and $f_2(y_2,\, y_A) = 0$, where $y_A$ denotes the dependency of the actual position and orientation of the solid axle. These equations are solved iteratively by the Newton-Algorithm. Starting with initial guesses $y_1^0$, $y_2^0$ one gets an improvement by solving the linear equations

$$\begin{aligned} \frac{\partial f_1}{\partial y_1}\, \left(y_1^{k+1} - y_1^k\right) &= -f_1(y_1\, y_A) \\ \frac{\partial f_2}{\partial y_2}\, \left(y_2^{k+1} - y_2^k\right) &= -f_2(y_2\, y_A) \end{aligned} \qquad k = 0, 1, 2, ... \tag{30}$$

Here, the Jacobians $\frac{\partial f_1}{\partial y_1}\, \frac{\partial f_2}{\partial y_2}$ can be calculated analytically.

### 3.5. Leaf Spring Reaction Forces

The actual forces in the front leaf eye bushing is given by

$$F_B \;=\; F_{0B} \;+\; c_B\, w_X \;+\; d_B\, \dot{u}_X \;, \tag{31}$$

where $F_{0B}$ is the pretension force and $c_B$, $d_B$ are 3×3 matrices, characterizing the stiffness and damping properties of the front leaf eye bushing. The displacement vector $w_X$ in the front leaf eye bushing depend on the generalized coordinates $y_1$ and $y_A$ which describe the actual shape of the front leaf spring part and the actual position and orientation of the solid axle. By solving Eq. (30) $y_1$ is given as a function of $(y_A)$. Hence, $w_x$ only depends on $y_A$ and its derivative can be calculated by

$$\dot{u}_X \;=\; \frac{\partial w_X}{\partial y_A}\, \dot{y}_A \;, \tag{32}$$

where $\dot{y}_A$ describes the velocity state of the solid axle.

The radial and lateral components of the shackle forces can be calculated from

$$F_{SR} \;=\; u_{SR}^T F_{0S} \;+\; c_{SR}\, w_{SR} \;+\; d_{SR}\, \dot{w}_{SR} \quad \text{and} \quad F_{SL} \;=\; u_{SL}^T F_{0S} \;+\; c_{SL}\, w_{SL} \;+\; d_{SL}\, \dot{w}_{SL} \;, \tag{33}$$

where $F_{0S}$ is the pretension force, $u_{SR}$, $u_{SL}$ are unit vectors in the radial and lateral shackle direction, and $c_{SR}$, $c_{SL}$, $d_{SR}$, $d_{SL}$ are constants, characterizing the stiffness and damping properties of the shackle. The shackle displacements $w_{SR}$ and $w_{SL}$ depend on the generalized coordinates $y_{2R}$ and $y_A$ which describe the actual shape of the rear leaf spring part and the actual position and orientation of the solid axle. Similar to Eq. (32) the displacement velocities are given by

$$\dot{u}_{SR} \;=\; \frac{\partial u_{SR}}{\partial y_A}\, \dot{y}_A \quad \text{and} \quad \dot{u}_{SL} \;=\; \frac{\partial u_{SL}}{\partial y_A}\, \dot{y}_A \;. \tag{34}$$

Finally the shackle force read as

$$F_S \;=\; F_{SR}\, u_{SR} \;+\; F_{SL}\, u_{SL} \;. \tag{35}$$

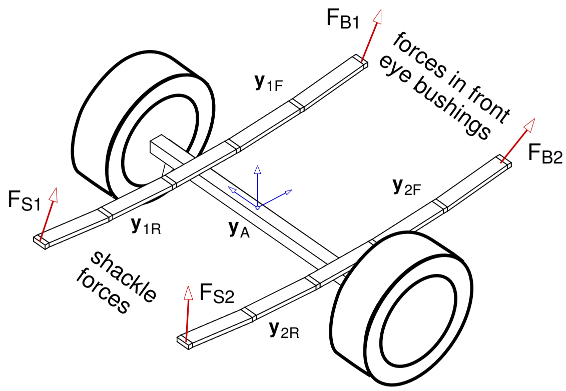


Figure 8: Forces Applied to Axle

### 3.6. Forces Applied to the Axle

In this approach the leaf springs act like generalized force elements, Fig. 8. Guidance and suspension of the solid axle is done by the resulting force

$$F \;=\; F_{B1} + F_{B2} + F_{S1} + F_{S2} \tag{36}$$

and the resulting torque

$$T \;=\; r_{AB1} \times F_{B1} + r_{AB2} \times F_{B2} + r_{AS1} \times F_{S1} + r_{AS2} \times F_{S2} \tag{37}$$

where $r_{AB1} = r_{AB1}(y_A)$, ... $r_{AS2}(y_A)$ describe the momentary position of the front eye bushings and the shackles relative to the axle center.

As the forces in the front eye bushings $F_{B1}$, $F_{B2}$ and the shackle forces $F_{S1}$, $F_{S2}$ depend on the axle state $y_A$, $\dot{y}_A$ only

$$F_{B1} = F_{B1}\left(y_a,\, \dot{y}_A\right)\;,\; F_{B2} = F_{B2}\left(y_a,\, \dot{y}_A\right)\;,\;\; F_{S1} = F_{B1}\left(y_a,\, \dot{y}_A\right)\;,\; F_{S2} = F_{B2}\left(y_a,\, \dot{y}_A\right)\;, \tag{38}$$

the resulting force $F$ and the resulting torque $T$ are also mere functions of the axle state.

As each leaf spring acts herby as a generalized force element it can easily be integrated into the vehicle framework. By suppressing high frequent leaf spring eigenmodes it is perfectly adopted to real-time application.

### 3.7. Bending Modes

The quasi-static approach reproduces all significant bending modes of the leaf spring, Fig.9.

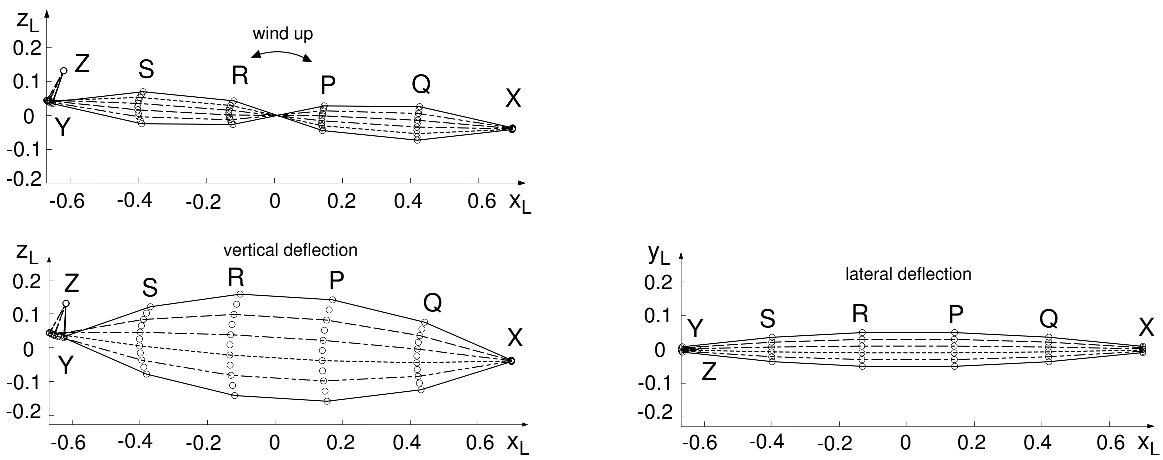


Figure 9: Bending Modes

A leaf spring is stiffer in the lateral direction than in the vertical direction. Hence, a displacement in the front eye bushing is noticeable only on lateral leaf spring deflections.

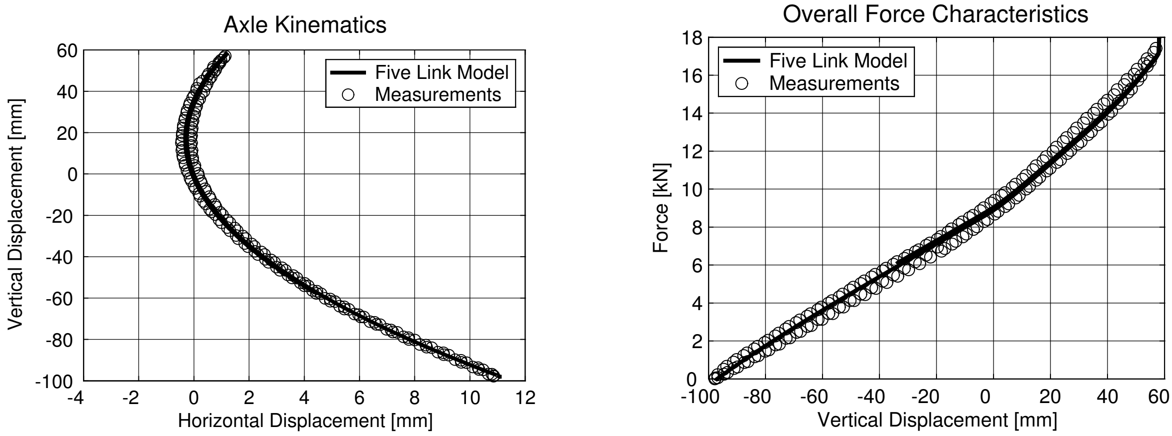


Figure 10: Comparison to Measurements

### 3.8. Model Performance

The five link leaf spring model was integrated into a ve-DYNA Ford Transit vehicle model. Using the five link leaf spring model at the rear axle instead of a poor kinematic approach means only 85% more computer run time. Hence, real time applications are still possible. The simulation results are in good conformity to measurements, Fig. 10. The nonlinearity in the spring characteristics is caused by an additional bump stop and by the change of the shackle position during jounce and rebound. Obviously the five link model is accurate enough.

## 4. Free Body Module

### 4.1. Position and Orientation

To describe the momentary state of the body $E$ the frame $x_E$ $y_E$, $z_E$ located in the center of gravity is used. In addition, sensor points $S$ monitor position, velocity and acceleration at specific body points, Fig. 11. The frame $B$ is fixed to the

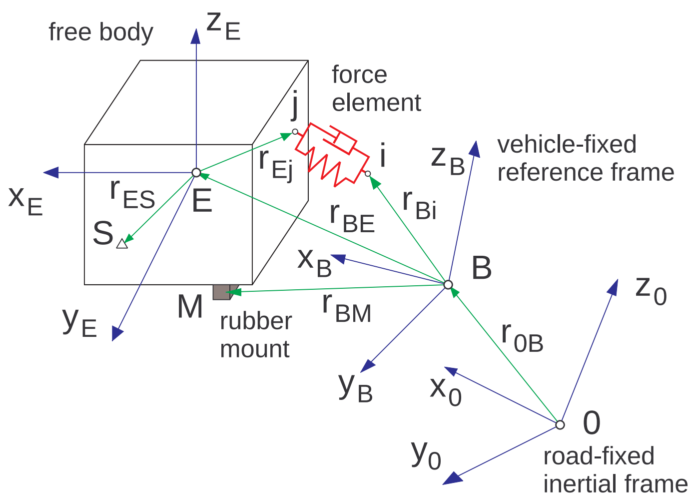


Figure 11: Elastically Suspended Body

vehicle. The suspension of body $E$ on the vehicle, frame $B$ may consist of force elements and/or rubber mounts. The road-fixed frame 0 is considered as inertial frame. The position of frame $B$ with respect to the road-fixed inertial frame 0 is given by the position vector

$$r_{0B,0} = \begin{bmatrix} x_B \\ y_B \\ z_B \end{bmatrix} . \tag{39}$$

The orientation of the frame axis are described by a rotation matrix. Three elementary rotations are put together. The sequence

$$A_{0B} = \underset{\text{yaw}}{A_{\gamma_B}} \; \underset{\text{pitch}}{A_{\beta_B}} \; \underset{\text{roll}}{A_{\alpha_B}} \tag{40}$$

results in

$$A_{0B} = \begin{bmatrix} \cos\beta_B \cos\gamma_B & \begin{matrix} -\cos\alpha_B \sin\gamma_B \\ +\sin\alpha_B \sin\beta_B \cos\gamma_B \end{matrix} & \begin{matrix} \sin\alpha_B \sin\gamma_B \\ +\cos\alpha_B \sin\beta_B \cos\gamma_B \end{matrix} \\ \cos\beta_B \sin\gamma_B & \begin{matrix} \cos\alpha_B \cos\gamma_B \\ +\sin\alpha_B \sin\beta_B \sin\gamma_B \end{matrix} & \begin{matrix} -\sin\alpha_B \cos\gamma_B \\ +\cos\alpha_B \sin\beta_B \sin\gamma_B \end{matrix} \\ -\sin\beta_B & \sin\alpha_B \cos\beta_B & \cos\alpha_B \cos\beta_B \end{bmatrix} . \tag{41}$$

Hence, position and orientation of the vehicle-fixed reference are described by 6 generalized coordinates $x_B, y_B, z_B$, and $\alpha_B, \beta_B, \gamma_B$.

The position and orientation of the elastically suspended body with respect to the reference frame $B$ is given by

$$r_{BE,B} = \begin{bmatrix} x_E \\ y_E \\ z_E \end{bmatrix} . \tag{42}$$

and

$$A_{BE} = \begin{bmatrix} 1 & 0 & 0 \\ 0 & \cos\alpha_E & -\sin\alpha_E \\ 0 & \sin\alpha_E & \cos\alpha_E \end{bmatrix} \begin{bmatrix} \cos\beta_E & 0 & \sin\beta_E \\ 0 & 1 & 0 \\ -\sin\beta_E & 0 & \cos\beta_E \end{bmatrix} \begin{bmatrix} \cos\gamma_E & -\sin\gamma_E & 0 \\ \sin\gamma_E & -\cos\gamma_E & 0 \\ 0 & 0 & 1 \end{bmatrix} . \tag{43}$$

### 4.2. Generalized Speeds

The velocity of the reference frame $B$ with respect to the inertial frame 0 is given by

$$v_{0B,0} = \dot{r}_{0B,0} = \begin{bmatrix} \dot{x}_B \\ \dot{y}_B \\ \dot{z}_B \end{bmatrix} \tag{44}$$

The velocity denoted in the inertial frame can be transformed to the reference frame

$$v_{0B,B} = A_{0B}^T \, \dot{r}_{0B,0} \, . \tag{45}$$

In doing so the orthogonality of the rotation matrix

$$A_{B0} = A_{0B}^{-1} = A_{0B}^T \tag{46}$$

was already taken into consideration.

The angular velocity of the reference frame $B$ with respect to the inertial frame 0 may be expressed directly in reference frame $B$

$$\omega_{0B,B} = \begin{bmatrix} 1 & 0 & -\sin\beta_B \\ 0 & \cos\alpha_B & \sin\alpha_B \cos\beta_B \\ 0 & -\sin\alpha_B & \cos\alpha_B \cos\beta_B \end{bmatrix} \begin{bmatrix} \dot{\alpha}_B \\ \dot{\beta}_B \\ \dot{\gamma}_B \end{bmatrix} . \tag{47}$$

The 6 components of $v_{0B,B}$ and $\omega_{0B,B}$ will now be chosen as generalized speeds. First order kinematical differential equations connect generalized speeds with derivatives of generalized coordinates. From Eq. 45 and Eq. 47 one gets

$$\begin{bmatrix} \dot{x}_B \\ \dot{y}_B \\ \dot{z}_B \end{bmatrix} = A_{0B} \begin{bmatrix} v_{0Bx} \\ v_{0By} \\ v_{0Bz} \end{bmatrix} . \tag{48}$$

and

$$\begin{bmatrix} 1 & 0 & -\sin\beta_B \\ 0 & \cos\alpha_B & \sin\alpha_B \cos\beta_B \\ 0 & -\sin\alpha_B & \cos\alpha_B \cos\beta_B \end{bmatrix} \begin{bmatrix} \dot{\alpha}_B \\ \dot{\beta}_B \\ \dot{\gamma}_B \end{bmatrix} = \begin{bmatrix} \omega_{0Bx} \\ \omega_{0By} \\ \omega_{0Bz} \end{bmatrix} . \tag{49}$$

Where the solution of Eq. 49 is given by

$$\begin{aligned} \dot{\gamma}_B &= (\omega_{0Bz} \cos\alpha_B + \omega_{0By} \sin\alpha_B) / \cos\beta_B \quad , \\ \dot{\beta}_B &= -\omega_{0Bz} \sin\alpha_B + \omega_{0By} \cos\alpha_B \quad , \\ \dot{\alpha}_B &= \omega_{0Bx} + \dot{\gamma}_B \, \cos\alpha_B \quad . \end{aligned} \tag{50}$$

The momentary state of the reference frame $B$ is fully characterized by 6 generalized coordinates $x_B$, $y_B$, $z_B$, $\alpha_B$, $\beta_B$, $\gamma_B$ and 6 generalized speeds $v_{0Bx}$, $v_{0By}$, $v_{0Bz}$, $\omega_{0Bx}$, $\omega_{0By}$, $\omega_{0Bz}$.

The velocity and the angular velocity of the elastically suspended body with respect to the inertia frame 0 is given by

$$\begin{aligned} v_{0E,B} &= v_{0B,B} + \omega_{0B,B} \times r_{BE,B} + \dot{r}_{BE,B} \,, \\ \omega_{0E,B} &= \omega_{0B,B} + \omega_{BE,B} \,, \end{aligned} \tag{51}$$

where the derivative of the position vector and the angular velocity of the elastically suspended body follow from Eq. 42 and Eq. 43. They read as

$$\dot{r}_{BE,B} = \begin{bmatrix} \dot{x}_E \\ \dot{y}_E \\ \dot{z}_E \end{bmatrix} \tag{52}$$

and

$$\omega_{BE,B} = \begin{bmatrix} 1 & 0 & \sin\beta_E \\ 0 & \cos\alpha_E & -\sin\alpha_E\cos\beta_E \\ 0 & \sin\alpha_E & \cos\alpha_E\cos\beta_E \end{bmatrix} \begin{bmatrix} \dot{\alpha}_E \\ \dot{\beta}_E \\ \dot{\gamma}_E \end{bmatrix} \tag{53}$$

By using the components of the velocity

$$v_{0E,B} = \begin{bmatrix} v_{0E_x} & v_{0E_y} & v_{0E_z} \end{bmatrix}^T \tag{54}$$

and the angular velocity

$$\omega_{0E,B} = \begin{bmatrix} \omega_{0E_x} & \omega_{0E_y} & \omega_{0E_z} \end{bmatrix}^T \tag{55}$$

as generalized speeds, Eq. 51 can be written as a set of kinematical differential equations

$$\begin{bmatrix} \dot{x}_E \\ \dot{y}_E \\ \dot{z}_E \end{bmatrix} = \begin{bmatrix} v_{0E_x} - v_{0B_x} \\ v_{0E_y} - v_{0B_y} \\ v_{0E_z} - v_{0B_z} \end{bmatrix} - \begin{bmatrix} \omega_{0E_x} \\ \omega_{0E_y} \\ \omega_{0E_z} \end{bmatrix} \times \begin{bmatrix} x_E \\ y_E \\ z_E \end{bmatrix} \tag{56}$$

$$\begin{bmatrix} 1 & 0 & \sin\beta_E \\ 0 & \cos\alpha_E & -\sin\alpha_E\cos\beta_E \\ 0 & \sin\alpha_E & \cos\alpha_E\cos\beta_E \end{bmatrix} \begin{bmatrix} \dot{\alpha}_E \\ \dot{\beta}_E \\ \dot{\gamma}_E \end{bmatrix} = \begin{bmatrix} \omega_{0E_x} - \omega_{0B_x} \\ \omega_{0E_y} - \omega_{0B_y} \\ \omega_{0E_z} - \omega_{0B_z} \end{bmatrix} \tag{57}$$

Whereas the 6 generalized coordinates $x_E$, $y_E$, $z_E$, $\alpha_E$, $\beta_E$, $\gamma_E$ describe the position and orientation of frame $E$ relative to frame $B$, the 6 generalized speeds $v_{0Ex}$, $v_{0Ey}$, $v_{0Ez}$, $\omega_{0Ex}$, $\omega_{0Ey}$, $\omega_{0Ez}$ are the components of the absolute velocity and angular velocity of body $E$.

### 4.3. Accelerations

The accelerations of body $E$ with respect to the inertia frame 0 can be expressed in reference frame $B$. They read as

$$\begin{aligned} a_{0E,B} &= \dot{v}_{0E,B} + \omega_{0B,B} \times v_{0E,B} \,, \\ \alpha_{0E,B} &= \dot{\omega}_{0E,B} + \omega_{0B,B} \times \omega_{0E,B} \,, \end{aligned} \tag{58}$$

where

$$\dot{v}_{0E,B} = \begin{bmatrix} \dot{v}_{0E_x} & \dot{v}_{0E_y} & \dot{v}_{0E_z} \end{bmatrix}^T \tag{59}$$

and

$$\dot{\omega}_{0E,B} = \begin{bmatrix} \dot{\omega}_{0E_x} & \dot{\omega}_{0E_y} & \dot{\omega}_{0E_z} \end{bmatrix}^T \tag{60}$$

follow from Eq. 54 and Eq. 55.

### 4.4. Force Elements

If a force element is attached to the chassis at point $i$ and to the body at point $j$ the momentary position of force element $ij$, is given by

$$r_{ij,B} = \underbrace{r_{BE,B} + r_{Ej,B}}_{r_{Bj,B}} - r_{Bi,K} \,, \tag{61}$$

where

$$r_{Ej,B} = A_{BE}\, r_{Ej,K} \,, \tag{62}$$

$r_{Bi,K}$, $r_{Ej,K}$ are given by data and $r_{BE,B}$ follows from Eq. (42).

The actual length can be calculated from

$$u^a_{ij} = \sqrt{r^T_{ij,B}\, r_{ij,B}} \,, \tag{63}$$

and the unit vector

$$e_{ij,B} = \frac{r_{ij,B}}{u^a_{ij}} \tag{64}$$

describes the momentary direction of the force element.

If $u^0_{ij}$ denotes the initial length of the force element, the displacement of the force element is given by

$$u_{ij} = u^0_{ij} - u^a_{ij} \,. \tag{65}$$

The displacement velocity follows from

$$v_{ij} = e^T_{ij,B} \frac{d}{dt} \left( r_{ij,B} \right) . \tag{66}$$

Using Eq. 61, Eq. 62, and $\dot{r}_{Bi,K} = 0$ one gets

$$v_{ij} = e^T_{ij,B} \left( \dot{r}_{BE,B} + \omega_{BE,B} \times r_{ej,B} \right) , \tag{67}$$

where $\dot{r}_{BE,B}$ and $\omega_{BE,B}$ are given by Eq. 52 and Eq. 53.

The forces $F_{ij,B}$, $F_{ji,B}$ and the torques $T_{ij,B}$, $T_{ji,B}$ applied to body and chassis are given by

$$F_{ij,B} = f(u_{ij},\, v_{ij})\; e_{ij,B} \,, \qquad F_{ji,B} = -F_{ij,B} \,, \tag{68}$$

and

$$T_{ij,B} = r_{Ej,B} \times F_{ij,B} \,, \qquad T_{ji,B} = r_{Bi,K} \times F_{ji,B} \,, \tag{69}$$

where $f$ describes an arbitrary spring/damper characteristics.

### 4.5. Equations of Motion

Applying liner and angular momentum to the elastically suspended body one gets

$$m_E\, \dot{v}_{0E,B} = F_{E,B} - m_E \left( g_{,B} + \omega_{0B,B} \times v_{0E,B} \right) \tag{70}$$

and

$$\Theta_{E,B}\, \dot{\omega}_{0E,B} = T_{E,B} - \omega_{0E,B} \times \Theta_{E,B} \omega_{0E,B} - \Theta_{E,B} \left( \omega_{0B,B} \times \omega_{0E,B} \right) , \tag{71}$$

where $m_E$, $\Theta_{E,B}$ denote mass and inertia tensor of the free body, $F_{E,B}$, $T_{E,B}$ are the resulting forces and torques applied to the free body, and $g_{,B}$ is the vector of gravity expressed in the body fixed reference frame. This equations are coupled with the chassis equations of motion only by the applied forces and torques. Due to the particular choose of generalized speeds no mass or inertia coupling terms appear.

By using this modelling technique, Seibert and Rill (1998) showed that the comfort of a passenger car is significantly influenced by the engine suspension system. The free body model can also be used to model an elastically suspended driver's cab, Rill (1993).

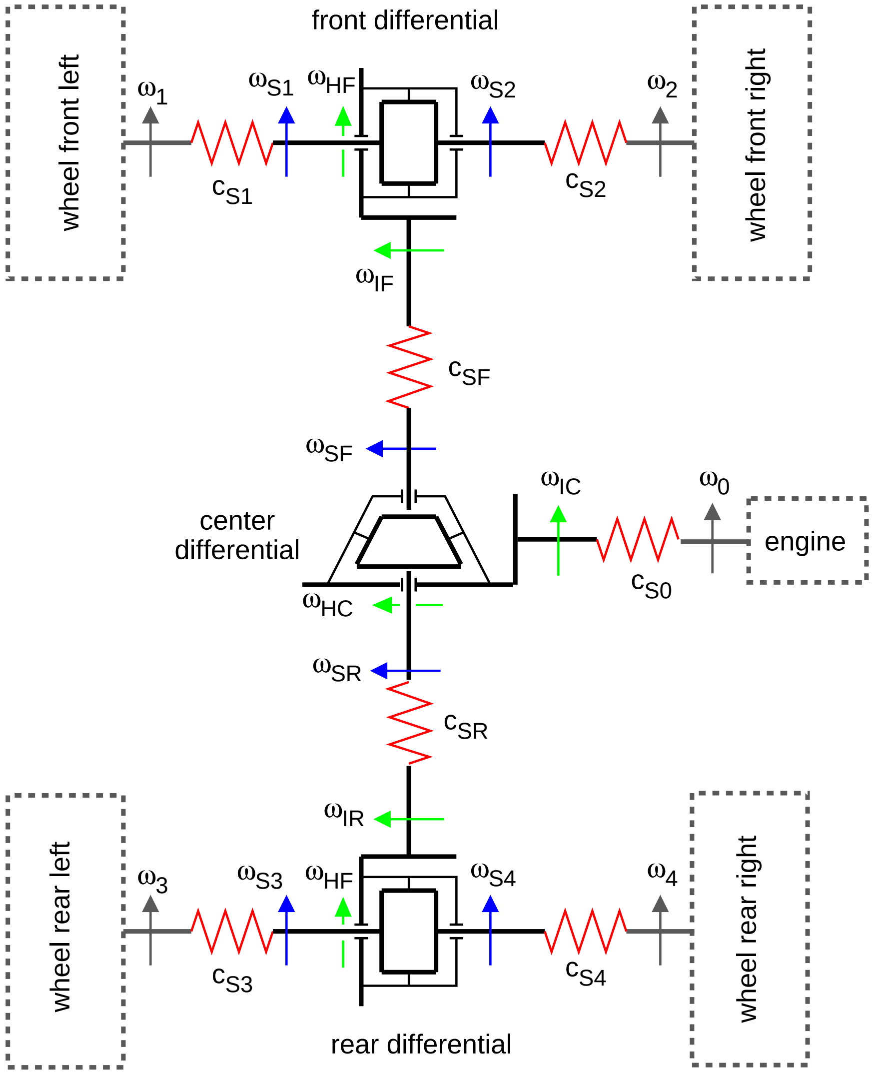


Figure 12: Drive Train Model

## 5. Subsystem Drive Train

### 5.1. Generic Model Structure

The subsystem drive train, Fig. 12, interact on one side with the engine and on the other side with the wheels. Hence, the angular velocities of the wheels $\omega_1, \ldots, \omega_4$, and the engine or respectively the gear output angular velocity $\omega_0$ are input quantities. That is why, the calculation of the engine torque and the dynamics of the wheel rotation are performed in other subsystems. Via the tire forces and torques the drive train is coupled with the steering system and the vehicle frame work.

The drive train model includes three lockable differentials. The angular velocities of the drive shafts $\omega_{S1}$: front left, $\omega_{S2}$: front right, $\omega_{SF}$: front, $\omega_{SR}$: rear, $\omega_{S3}$: rear left, $\omega_{S4}$: rear right are used as generalized coordinates.

The torque distribution of the front and rear differential is 1:1. If $r_F$ and $r_R$ are the ratios of the front and rear differential then one gets

$$\begin{aligned} \omega_{HF} &= \tfrac{1}{2}\,\omega_{S1} + \tfrac{1}{2}\,\omega_{S2}\,, \\ \omega_{IF} &= r_F\,\omega_{HF}\,; \end{aligned} \tag{72}$$

$$\begin{aligned} \omega_{HR} &= \tfrac{1}{2}\,\omega_{S3} + \tfrac{1}{2}\,\omega_{S4}\,, \\ \omega_{IR} &= r_R\,\omega_{HR}\,. \end{aligned} \tag{73}$$

The torque distribution of the center differential is given by

$$\frac{t_F}{t_R} = \frac{\mu}{1-\mu}\,, \tag{74}$$

where $t_F$, $t_R$ denote the torques transmitted to the front and rear drive shaft, and $\mu$ is a dimensionless drive train parameter. A value of $\mu = 1$ means front wheel drive, $0 < \mu < 1$ stands for all wheel drive, and $\mu = 0$ is rear wheel drive. If the ratio of the center differential is given by $r_C$ then

$$\begin{aligned} \omega_{HC} &= \mu\,\omega_{SF} + (1-\mu)\,\omega_{SR} \\ \omega_{IC} &= r_C\,\omega_{HC} \end{aligned} \tag{75}$$

holds.

### 5.2. Equation of Motion

The equation of motion for the drive train is derived from Jordain's Principle, which for the drive train reads as

$$\sum \left( \Theta_i\,\dot\omega_i - t_i \right) \delta\,\omega_i \;=\; 0\,, \tag{76}$$

where $\Theta_i$ is the inertia of body $i$, $\dot\omega_i$ denotes the time derivatives of the angular velocity, $t_i$ is the torque applied to each body, and $\delta\,\omega_i$ describe the variation of the angular velocity. Applying Eq. (76) for the different parts of the drive train model results in

$$\begin{aligned} \text{front drive shaft left:} \quad & \left( \Theta_{S1}\,\dot\omega_{S1} - t_{S1} - t_{LF} \right) \delta\,\omega_{S1} \;=\; 0\,, \\ \text{front drive shaft right:} \quad & \left( \Theta_{S2}\,\dot\omega_{S2} - t_{S2} + t_{LF} \right) \delta\,\omega_{S2} \;=\; 0\,, \\ \text{front differential housing:} \quad & \left( \Theta_{HF}\,\dot\omega_{HF} \right) \delta\,\omega_{HF} \;=\; 0\,, \\ \text{front differential input shaft:} \quad & \left( \Theta_{IF}\,\dot\omega_{IF} + t_{SF} \right) \delta\,\omega_{IF} \;=\; 0\,, \end{aligned} \tag{77}$$

$$\begin{aligned} \text{front drive shaft:} \quad & \left( \Theta_{SF}\,\dot\omega_{SF} - t_{SF} - t_{LC} \right) \delta\,\omega_{SF} \;=\; 0\,, \\ \text{rear drive shaft:} \quad & \left( \Theta_{SR}\,\dot\omega_{SR} - t_{SR} + t_{LC} \right) \delta\,\omega_{SR} \;=\; 0\,, \\ \text{center differential housing:} \quad & \left( \Theta_{HC}\,\dot\omega_{HC} \right) \delta\,\omega_{HC} \;=\; 0\,, \\ \text{center differential input shaft:} \quad & \left( \Theta_{IC}\,\dot\omega_{IC} + t_{S0} \right) \delta\,\omega_{IC} \;=\; 0\,, \end{aligned} \tag{78}$$

$$\begin{aligned} \text{rear differential input shaft:} \quad & \left( \Theta_{IR}\,\dot\omega_{IR} + t_{SR} \right) \delta\,\omega_{IR} \;=\; 0\,, \\ \text{rear differential housing:} \quad & \left( \Theta_{HR}\,\dot\omega_{HR} \right) \delta\,\omega_{HR} \;=\; 0\,, \\ \text{rear drive shaft left:} \quad & \left( \Theta_{S3}\,\dot\omega_{S3} - t_{S3} - t_{LR} \right) \delta\,\omega_{S3} \;=\; 0\,, \\ \text{rear drive shaft right:} \quad & \left( \Theta_{S4}\,\dot\omega_{S4} - t_{S4} + t_{LR} \right) \delta\,\omega_{S4} \;=\; 0\,. \end{aligned} \tag{79}$$

Using Eq. (72), Eq. (75), and Eq. (73) one gets

$$\begin{aligned} \Big(\Theta_{S1}\,\dot\omega_{S1} - t_{S1} - t_{LF}\Big)\,\delta\,\omega_{S1} &= 0\,, \\ \Big(\Theta_{S2}\,\dot\omega_{S2} - t_{S2} + t_{LF}\Big)\,\delta\,\omega_{S2} &= 0\,, \\ \Big(\Theta_{HF}\,\left(\tfrac12\,\dot\omega_{S1} + \tfrac12\,\dot\omega_{S2}\right)\Big)\Big(\tfrac12\,\delta\,\omega_{S1} + \tfrac12\,\delta\,\omega_{S2}\Big) &= 0\,, \\ \Big(\Theta_{IF}\,\left(\tfrac12\,r_F\,\dot\omega_{S1} + \tfrac12\,r_F\,\dot\omega_{S2}\right) + t_{SF}\Big)\Big(\tfrac12\,r_F\,\delta\,\omega_{S1} + \tfrac12\,r_F\,\delta\,\omega_{S2}\Big) &= 0\,, \\ \Big(\Theta_{SF}\,\dot\omega_{SF} - t_{SF} - t_{LC}\Big)\,\delta\,\omega_{SF} &= 0\,, \\ \Big(\Theta_{SR}\,\dot\omega_{SR} - t_{SR} + t_{LC}\Big)\,\delta\,\omega_{SR} &= 0\,, \\ \Big(\Theta_{HC}\,\left(\mu\,\dot\omega_{SF} + (1-\mu)\,\dot\omega_{SR}\right)\Big)\Big(\mu\,\delta\,\omega_{SF} + (1-\mu)\,\delta\,\omega_{SR}\Big) &= 0\,, \\ \Big(\Theta_{IC}\,\left(\mu\,r_C\,\dot\omega_{SF} + (1-\mu)\,r_C\,\dot\omega_{SR}\right) + t_{S0}\Big)\Big(\mu\,r_C\,\delta\,\omega_{SF} + (1-\mu)\,r_C\,\delta\,\omega_{SR}\Big) &= 0\,, \\ \Big(\Theta_{IR}\,\left(\tfrac12\,r_R\,\dot\omega_{S3} + \tfrac12\,r_R\,\dot\omega_{S4}\right) + t_{SR}\Big)\Big(\tfrac12\,r_R\,\delta\,\omega_{S3} + \tfrac12\,r_R\,\delta\,\omega_{S4}\Big) &= 0\,, \\ \Big(\Theta_{HR}\,\left(\tfrac12\,\dot\omega_{S3} + \tfrac12\,\dot\omega_{S4}\right)\Big)\Big(\tfrac12\,\delta\,\omega_{S3} + \tfrac12\,\delta\,\omega_{S4}\Big) &= 0\,, \\ \Big(\Theta_{S3}\,\dot\omega_{S3} - t_{S3} - t_{LR}\Big)\,\delta\,\omega_{S3} &= 0\,, \\ \Big(\Theta_{S4}\,\dot\omega_{S4} - t_{S4} + t_{LR}\Big)\,\delta\,\omega_{S4} &= 0\,. \end{aligned} \tag{80}$$

Collecting all terms with $\delta\,\omega_{S1}$, $\delta\,\omega_{S2}$, $\delta\,\omega_{SF}$, $\delta\,\omega_{SR}$, $\delta\,\omega_{S3}$, $\delta\,\omega_{S4}$ and using the abbreviation $\nu = 1-\mu$ one finally gets three blocks of differential equations

$$\begin{aligned}
&\big(\Theta_{S1}+\tfrac{1}{4}\,\Theta_{HF}+\tfrac{1}{4}\,r_F^2\,\Theta_{IF}\big)\,\dot\omega_{S1} + \big(\tfrac{1}{4}\,\Theta_{HF}+\tfrac{1}{4}\,r_F^2\,\Theta_{IF}\big)\,\dot\omega_{S2} = t_{S1} + t_{LF} - \tfrac{1}{2}\,r_F\,t_{SF}\ ,\\
&\big(\tfrac{1}{4}\,\Theta_{HF}+\tfrac{1}{4}\,r_F^2\,\Theta_{IF}\big)\,\dot\omega_{S1} + \big(\Theta_{S2}+\tfrac{1}{4}\,\Theta_{HF}+\tfrac{1}{4}\,r_F^2\,\Theta_{IF}\big)\,\dot\omega_{S2} = t_{S2} - t_{LF} - \tfrac{1}{2}\,r_F\,t_{SF}\ ,
\end{aligned} \tag{81}$$

$$\begin{aligned}
&\big(\Theta_{SF}+\mu^2\,\Theta_{HC}+\mu^2\,r_C^2\,\Theta_{IC}\big)\,\dot\omega_{SF} + \big(\mu\,\nu\,\Theta_{HC}+\mu\,\nu\,r_C^2\,\Theta_{IC}\big)\,\dot\omega_{SR} = t_{SF} + t_{LC} - \mu\,r_C\,t_{S0}\ ,\\
&\big(\mu\,\nu\,\Theta_{HC}+\mu\,\nu\,r_C^2\,\Theta_{IC}\big)\,\dot\omega_{SF} + \big(\Theta_{SR}+\nu^2\,\Theta_{HC}+\nu^2\,r_C^2\,\Theta_{IC}\big)\,\dot\omega_{SR} = t_{SR} - t_{LC} - \nu\,r_C\,t_{S0}\ ,
\end{aligned} \tag{82}$$

$$\begin{aligned}
&\big(\Theta_{S3}+\tfrac{1}{4}\,\Theta_{HR}+\tfrac{1}{4}\,r_R^2\,\Theta_{IR}\big)\,\dot\omega_{S3} + \big(\tfrac{1}{4}\,\Theta_{HR}+\tfrac{1}{4}\,r_R^2\,\Theta_{IR}\big)\,\dot\omega_{S4} = t_{S3} + t_{LR} - \tfrac{1}{2}\,r_R\,t_{SR}\ ,\\
&\big(\tfrac{1}{4}\,\Theta_{HR}+\tfrac{1}{4}\,r_R^2\,\Theta_{IR}\big)\,\dot\omega_{S3} + \big(\Theta_{S4}+\tfrac{1}{4}\,\Theta_{HR}+\tfrac{1}{4}\,r_R^2\,\Theta_{IR}\big)\,\dot\omega_{S4} = t_{S4} - t_{LR} - \tfrac{1}{2}\,r_R\,t_{SR}\ ,
\end{aligned} \tag{83}$$

which describe the dynamics of the drive train. Due to its simple structure an extension to a $4{\times}4$-drive train will be straight forward.

### 5.3. Drive Shaft Torques

The torques in the drive shafts are given by

$$\begin{aligned}
t_{S1} &= c_{S1}\,\triangle\varphi_{S1}\,, &\text{where:}\quad \triangle\dot\varphi_{S1} &= \omega_1 - \omega_{S1}\,;\\
t_{S2} &= c_{S2}\,\triangle\varphi_{S2}\,, &\text{where:}\quad \triangle\dot\varphi_{S2} &= \omega_2 - \omega_{S2}\,;\\
t_{SF} &= c_{SF}\,\triangle\varphi_{SF}\,, &\text{where:}\quad \triangle\dot\varphi_{SF} &= \omega_{IF} - \omega_{SF}\,;\\
t_{S0} &= c_{S0}\,\triangle\varphi_{S0}\,, &\text{where:}\quad \triangle\dot\varphi_{S0} &= \omega_{IC} - \omega_0\,;\\
t_{SR} &= c_{SR}\,\triangle\varphi_{SR}\,, &\text{where:}\quad \triangle\dot\varphi_{SR} &= \omega_{IR} - \omega_{SR}\,;\\
t_{S3} &= c_{S3}\,\triangle\varphi_{S3}\,, &\text{where:}\quad \triangle\dot\varphi_{S3} &= \omega_3 - \omega_{S3}\,;\\
t_{S4} &= c_{S4}\,\triangle\varphi_{S4}\,, &\text{where:}\quad \triangle\dot\varphi_{S4} &= \omega_4 - \omega_{S4}\,;
\end{aligned} \tag{84}$$

and $c_{S0}$, $c_{S1}$, $c_{S2}$, $c_{S3}$, $c_{S4}$, $c_{SF}$, $c_{SR}$ denote the stiffness of the drive shafts. The first order differential equations can be arranged in matrix form

$$\triangle\dot\varphi = K\,\omega + \Omega_0\,, \tag{85}$$

where

$$\omega = \big[\ \omega_{S1},\ \ \omega_{S2},\ \ \omega_{SF},\ \ \omega_{SR},\ \ \omega_{S3},\ \ \omega_{S4}\ \big]^T \tag{86}$$

is the vector of the angular velocities,

$$\triangle\varphi = \big[\ \triangle\varphi_{S1},\ \ \triangle\varphi_{S2},\ \ \triangle\varphi_{SF},\ \ \triangle\varphi_{S0},\ \ \triangle\varphi_{SR},\ \ \triangle\varphi_{S3},\ \ \triangle\varphi_{S4}\ \big]^T \tag{87}$$

contains the torsional angles in the drive shafts,

$$\Omega_0 = \big[\ \omega_1,\ \ \omega_2,\ \ 0,\ \ -\omega_0,\ \ 0,\ \ \omega_3,\ \ \omega_4\ \big]^T \tag{88}$$

is the excitation vector, and

$$K = \begin{bmatrix}
-1 & 0 & 0 & 0 & 0 & 0\\
0 & -1 & 0 & 0 & 0 & 0\\
\tfrac{1}{2}\,r_F & \tfrac{1}{2}\,r_F & -1 & 0 & 0 & 0\\
0 & 0 & \mu\,r_C & (1-\mu)\,r_C & 0 & 0\\
0 & 0 & 0 & -1 & \tfrac{1}{2}\,r_R & \tfrac{1}{2}\,r_R\\
0 & 0 & 0 & 0 & -1 & 0\\
0 & 0 & 0 & 0 & 0 & -1
\end{bmatrix} \tag{89}$$

is a $7{\times}6$ distribution matrix.

### 5.4. Locking Torques

The differential locking torques are modelled by an enhanced dry friction model consisting of a static and a dynamic part

$$\begin{aligned} t_{LF} &= t_{LF}^S + t_{LF}^D \,, \\ t_{LC} &= t_{LC}^S + t_{LC}^D \,, \\ t_{LR} &= t_{LR}^S + t_{LR}^D \,. \end{aligned} \tag{90}$$

The dynamic parts are modelled by a torque proportional to the differential output angular velocities

$$\begin{aligned} t_{LF}^D &= d_{LF}\left(\omega_{S2} - \omega_{S1}\right) \,, \\ t_{LC}^D &= d_{LC}\left(\omega_{SR} - \omega_{SF}\right) \,, \,, \\ t_{LR}^D &= d_{LR}\left(\omega_{S4} - \omega_{S3}\right) \end{aligned} \tag{91}$$

where $d_{LF}, d_{LC}, d_{LR}$ are damping parameters which have to be chosen appropriately. In steady state operating conditions the static parts $t_{LF}^S$, $t_{LC}^S$, $t_{LR}^S$ will provide torques even if the differential output angular velocities are equal. From Eq. (81), Eq. (82), Eq. (83), one gets

$$\begin{aligned} t_{LF}^D &= \tfrac{1}{2}\left(\, t_{S2} - t_{S1} \,\right) \,, \\ t_{LF}^D &= \tfrac{1}{2}\left(\, t_{SR} - t_{SF} + (2\mu - 1)\, r_C\, t_{S0} \,\right) \,, \\ t_{LR}^D &= \tfrac{1}{2}\left(\, t_{S4} - t_{S3} \,\right) \,. \end{aligned} \tag{92}$$

By this locking torque model the effect of dry friction inside the differentials can also be taken into account.

### 5.5. Numerical Solution

The equations of motion Eq. (81), Eq. (82), and Eq. (83) can be combined in a matrix differential equation

$$M\,\dot\omega \;=\; q(\triangle\varphi,\, \omega)\,, \tag{93}$$

where $\omega$, $\triangle\varphi$ are given by Eq. (86), Eq. (87) and the mass matrix $M$ is built by three $2\times 2$ submatrices

$$M \;=\; \begin{bmatrix} M_F & 0 & 0 \\ 0 & M_C & 0 \\ 0 & 0 & M_R \end{bmatrix}\,, \tag{94}$$

where the elements of $M_F$, $M_c$, and $M_R$ follow from Eq. (81), Eq. (82), and Eq. (83). The vector of the generalized torques is given by

$$q \;=\; \begin{bmatrix} t_{S1} + t_{LF} - \frac{1}{2}\, r_F\, t_{SF} \\ t_{S2} - t_{LF} - \frac{1}{2}\, r_F\, t_{SF} \\ t_{SF} + t_{LC} - \mu\, r_C\, t_{S0} \\ t_{SR} - t_{LC} - (1-\mu)\, r_C\, t_{S0} \\ t_{S3} + t_{LR} - \frac{1}{2}\, r_R\, t_{SR} \\ t_{S4} - t_{LR} - \frac{1}{2}\, r_R\, t_{SR} \end{bmatrix}\,. \tag{95}$$

Because the model also includes the high frequent drive shaft vibrations the differential equations for the drive train are stiff. Hence, implicit integration algorithm should be used for the numerical solution. Vehicle dynamic equations can be solved very effectively by a modified implicit Euler algorithm, Rill (2004).

The implicit Euler-Formalism for Eq. (93) and Eq. (85) results in

$$M\,\omega^{k+1} \;=\; M\,\omega^{k} \;+\; h\, q\left(\triangle\varphi^{k+1},\, \omega^{k+1}\right)\,, \tag{96}$$

$$\triangle\varphi^{k+1} \;=\; \triangle\varphi^{k} \;+\; h\,\left(K\,\omega^{k+1} \;+\; \Omega_0\right)\,, \tag{97}$$

where $h$ is the integration step size, and the superscripts ${}^{k}$ and ${}^{k+1}$ indicate the states at $t$ and $t+h$. Applying the Taylor-Expansion to $q$ at $\triangle\varphi^k + h\,\triangle\dot\varphi^k$ and $\omega^k$ one gets

$$\begin{aligned} q\left(\triangle\varphi^{k+1},\, \omega^{k+1}\right) \;\approx\;& q\left(\triangle\varphi^{k} + h\,\triangle\dot\varphi^{k},\, \omega^{k}\right) \\ +\;& \frac{\partial q}{\partial\triangle\varphi}\left(\triangle\varphi^{k+1} - \left(\triangle\varphi^{k} + h\,\triangle\dot\varphi^{k}\right)\right) \\ +\;& \frac{\partial q}{\partial\omega}\left(\omega^{k+1} - \omega^{k}\right) \end{aligned}\,. \tag{98}$$

By using Eq. (85) and Eq. (97) the second term on the right side can be written as

$$
\begin{aligned}
\frac{\partial q}{\partial \triangle\varphi}\left(\triangle\varphi^{k+1}-\left(\triangle\varphi^{k}+h\,\triangle\dot{\varphi}^{k}\right)\right) &= \frac{\partial q}{\partial \triangle\varphi}\left(\triangle\varphi^{k+1}-\triangle\varphi^{k} \quad - \quad h\,\triangle\dot{\varphi}^{k} \quad\right) \\
&= \frac{\partial q}{\partial \triangle\varphi}\left(h\,\left(K\,\omega^{k+1}+\Omega_0\right)-h\,\left(K\,\omega^{k}+\Omega_0\right)\right) \\
&= h\,\frac{\partial q}{\partial \triangle\varphi}\,K\left(\omega^{k+1}-\omega^{k}\right).
\end{aligned}
\tag{99}
$$

Now, the implicit algorithm in Eq. (96) can be approximated by

$$
M\,\omega^{k+1} \;=\; M\,\omega^{k} \;+\; h\,q\left(\triangle\varphi^{k}+h\triangle\dot{\varphi}^{k},\,\omega^{k}\right) \;+\; h\,\left(\frac{\partial q}{\partial \triangle\varphi}\,K\,+\frac{\partial q}{\partial \omega}\right)\left(\omega^{k+1}-\omega^{k}\right), \tag{100}
$$

which finally results in

$$
\omega^{k+1} \;=\; \omega^{k} \;+\; h\,\left(M-\frac{\partial q}{\partial \triangle\varphi}\,K\,-\frac{\partial q}{\partial \omega}\right)^{-1} q\left(\triangle\varphi^{k}+h\triangle\dot{\varphi}^{k},\,\omega^{k}\right)\;, \tag{101}
$$

where the partial derivatives $\partial q/\partial\triangle\varphi$ and $\partial q/\partial\omega$ can be calculated quite easily.

### 5.6. Partial Derivatives

Only the dynamic locking torques $t^D_{LF}$, $t^D_{LC}$ and $t^D_{LR}$ depend on the angular velocities. Hence, one gets

$$
\frac{\partial q}{\partial \omega} = \begin{bmatrix}
-d_{LF} & d_{LF} & 0 & 0 & 0 & 0 \\
d_{LF} & -d_{LF} & 0 & 0 & 0 & 0 \\
0 & 0 & -d_{LC} & d_{LC} & 0 & 0 \\
0 & 0 & d_{LC} & -d_{LC} & 0 & 0 \\
0 & 0 & 0 & 0 & -d_{LR} & d_{LR} \\
0 & 0 & 0 & 0 & d_{LR} & -d_{LR}
\end{bmatrix}. \tag{102}
$$

The change of $q$ with respect to $\triangle\varphi$ leads to a $6\times 7$ matrix

$$
\frac{\partial q}{\partial \triangle\varphi} = \begin{bmatrix}
c_{S1} & 0 & -\frac{1}{2}\,r_F\,c_{SF} & 0 & 0 & 0 & 0 \\
0 & c_{S2} & -\frac{1}{2}\,r_F\,c_{SF} & 0 & 0 & 0 & 0 \\
0 & 0 & c_{SF} & -\mu\,r_C\,c_{S0} & 0 & 0 & 0 \\
0 & 0 & 0 & -(1-\mu)\,r_C\,c_{S0} & c_{SR} & 0 & 0 \\
0 & 0 & 0 & 0 & -\frac{1}{2}\,r_R\,c_{SR} & c_{S3} & 0 \\
0 & 0 & 0 & 0 & -\frac{1}{2}\,r_R\,c_{SR} & 0 & c_{S3}
\end{bmatrix}. \tag{103}
$$

The term which is finally needed in Eq. (101) is symmetric and reads as

$$
\frac{\partial q}{\partial \triangle\varphi}\,K = \begin{bmatrix}
-c^*_{S1} & -\frac{1}{4}\,r_F^2\,c_{SF} & \frac{1}{2}\,r_F\,c_{SF} & 0 & 0 & 0 \\
-\frac{1}{4}\,r_F^2\,c_{SF} & -c^*_{S2} & \frac{1}{2}\,r_F\,c_{SF} & 0 & 0 & 0 \\
\frac{1}{2}\,r_F\,c_{SF} & \frac{1}{2}\,r_F\,c_{SF} & -c^*_{SF} & -\mu\,\widetilde{\mu}\,r_C^2\,c_{S0} & 0 & 0 \\
0 & 0 & -\mu\,\widetilde{\mu}\,r_C^2\,c_{S0} & -c^*_{SR} & \frac{1}{2}\,r_F\,c_{SF} & \frac{1}{2}\,r_F\,c_{SF} \\
0 & 0 & 0 & \frac{1}{2}\,r_R\,c_{SR} & -c_{S3} & -\frac{1}{4}\,r_R^2\,c_{SR} \\
0 & 0 & 0 & \frac{1}{2}\,r_R\,c_{SR} & -\frac{1}{4}\,r_R^2\,c_{SR} & -c_{S4}
\end{bmatrix}, \tag{104}
$$

where the abbreviations $\widetilde{\mu} = 1-\mu$, and

$$
\begin{aligned}
c^*_{S1} &= c_{S1}+\tfrac{1}{4}\,r_F^2\,c_{SF}\,, & c^*_{S2} &= c_{S2}+\tfrac{1}{4}\,r_F^2\,c_{SF}\,, \\
c^*_{SF} &= c_{SF}+\mu^2\,r_C^2\,c_{S0}\,, & c^*_{SR} &= c_{SR}+\widetilde{\mu}^2\,r_C^2\,c_{S0}\,, \\
c^*_{S3} &= c_{S3}+\tfrac{1}{4}\,r_r^2\,c_{SR}\,, & c^*_{S4} &= c_{S4}+\tfrac{1}{4}\,r_r^2\,c_{SR}
\end{aligned}
\tag{105}
$$

were used.

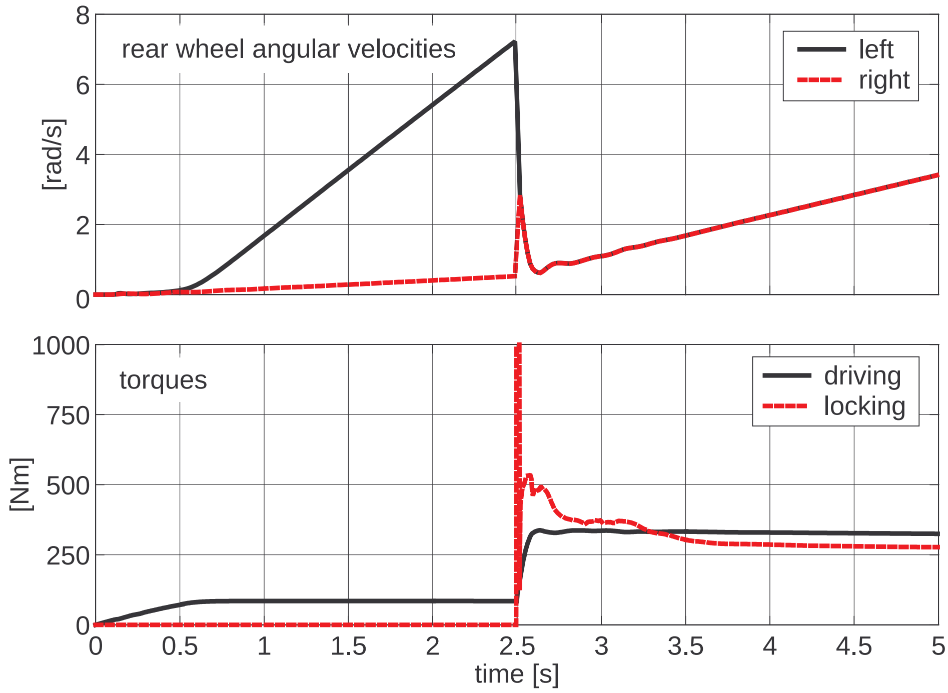


Figure 13: Vehicle starting on $\mu$-split

### 5.7. System Performance

Locking the differential improves the traction of a vehicle. In Fig. 13 the simulation results of a vehicle with rear wheel drive starting on a $\mu$-split surface are shown. At first all differentials are unlocked. The left rear wheel which is running on a low $\mu$-plate immediately starts to spin. At $t = 2.5\ s$ the rear differential is locked. Now, the locking torque which is generated by the drive train model forces both wheels to run with the same angular velocity.

## 6. Conclusion

Vehicle modelling by subsystems make a large variety of applications possible. The Combination of simple subsystems and modules results in a vehicle model with a minimum number of data and a very good run time performance. Such ”light models” can be used to develop an enhance control strategies for electronic safety devices. Depending on the focus of interest more and more subsystems and modules may be replaced by enhanced ones. Then, sophisticated design studies or a comfort analysis are possible. If the modified implicit Euler algorithm is also applied to the critical subsystems drive train and steering system the numerical solution of the overall vehicle model is still not time consuming.

## 7. References


ADAMS/Chassis 12.0 Reference Guide.

Fickers, P.; Richter, B.: Incorporating FEA-Techniques into MSA illustrated by several Rear Suspension Concepts. In: 9th European ADAMS User Conference, Frankfurt, November 21st/22nd, 1994.

Gipser, M.: Reifenmodelle für Komfort- und Schlechtwegsimulationen. In: Tagungsband zum 7. Aachener Kolloquium Fahrzeug- und Motorentechnik. IKA, RWTH Aachen und VDI 1998.

Hirschberg, W.; Rill, G.; Weinfurter, H.: User-Appropriate Tyre-Modelling for Vehicle Dynamics in Standard and Limit Situations. Vehicle System Dynamics 2002, Vol. 38, No. 2, pp. 103-125. Lisse: Swets & Zeitlinger.

van der Jagt, P.: The Road to Virtual Vehicle Prototyping; new CAE-models for accelerated vehicle dynamics development. PhD-Tesis, Tech. Univ. Eindhofen, Eindhofen 2000, ISBN 90-386-2552-9 NUGI 834.

Matschinsky, W.: Radführungen der Straßenfahrzeuge. Springer, Berlin 1998.

Rill, G.: Demands on Vehicle Modelling. In: The Dynamics of Vehicles on Road and on Tracks. Ed.: Anderson, R.J., Lisse: Swets-Zeitlinger 1990.

Rill, G.; Rauh, J.: Simulation von Tankfahrzeugen. In: Berechnung im Automobilbau, VDI-Bericht 1007. Düsseldorf: VDI-Verlag 1992.

Rill, G.: Modeling and Dynamic Optimization of Heavy Agricultural Tractors. In: 26th International Symposium on Automotive Technology and Automation (ISATA). Croydon: Automotive Automation Limited 1993.

Rill, G.: Simulation von Kraftfahrzeugen. Vieweg, Braunschweig 1994.

Rill, G.: Seibert, Th.; Rill, G.: Fahrkomfortberechnungen unter Einbeziehung der Motorschwingungen. In: Berechnung und Simulation im Fahrzeugbau, VDI-Bericht 1411. Düsseldorf: VDI-Verlag 1998.

Rill, G.: A Modified Implicit Euler Algorithm for Solving Vehicle Dynamics Equation. To Appear In: Multibody System Dynamics, 2004.

Tesis: www.tesis.de.